

Electrochemically Scalable Production of Fluorine-Modified Graphene for Flexible and High-Energy Ionogel-Based Microsupercapacitors

Feng Zhou,[†] Haibo Huang,[†] Chuanhai Xiao,^{†,‡} Shuanghao Zheng,^{†,‡,§} Xiaoyu Shi,^{†,‡,||} Jieqiong Qin,^{†,§} Qiang Fu,^{†,‡,||} Xinhe Bao,^{†,‡,||} Xinliang Feng,^{*,†,||} Klaus Müllen,^{*,†,||} and Zhong-Shuai Wu^{*,†,||}

[†]Dalian National Laboratory for Clean Energy, Dalian Institute of Chemical Physics, Chinese Academy of Sciences, 457 Zhongshan Road, Dalian 116023, China

[‡]State Key Laboratory of Catalysis, Dalian Institute of Chemical Physics, Chinese Academy of Sciences, 457 Zhongshan Road, Dalian 116023, China

[§]University of Chinese Academy of Sciences, 19 A Yuquan Road, Shijingshan District, Beijing 100049, China

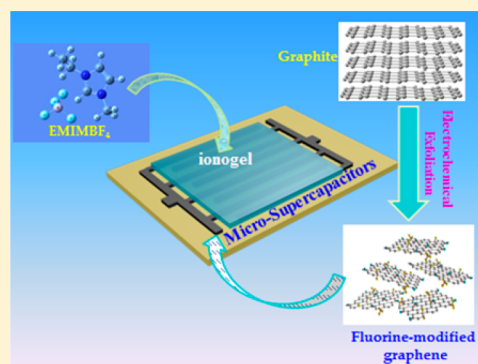
^{||}Department of Chemical Physics, University of Science and Technology of China, 96 JinZhai Road, Hefei 230026, P. R. China

[⊥]Center for Advancing Electronics Dresden (cfaed) & Department of Chemistry and Food Chemistry, Technische Universität Dresden, Mommsenstraße 4, 01062 Dresden, Germany

[¶]Max-Planck-Institut für Polymerforschung, Ackermannweg 10, 55128 Mainz, Germany

Supporting Information

ABSTRACT: Scalable production of high-quality heteroatom-modified graphene is critical for microscale supercapacitors but remains a great challenge. Herein, we demonstrate a scalable, single-step electrochemical exfoliation of graphite into highly solution-processable fluorine-modified graphene (FG), achieved in an aqueous fluorine-containing neutral electrolyte, for flexible and high-energy-density ionogel-based microsupercapacitors (FG-MSCs). The electrochemically exfoliated FG nanosheets are characterized by atomic thinness, large lateral size (up to 12 μm), a high yield of >70% with ≤ 3 layers, and a fluorine doping of 3 at%, allowing for large-scale production of FG-MSCs. Our ionogel-based FG-MSCs deliver high energy density of 56 mWh cm^{-3} , by far outperforming the most reported MSCs. Furthermore, the all-solid-state microdevices offer exceptional cyclability with $\sim 93\%$ after 5000 cycles, robust mechanical flexibility with 100% of capacitance retention bended at 180° , and outstanding serial and parallel integration without the requirement of metal-based interconnects for high-voltage and high-capacitance output. Therefore, these FG-MSCs represent remarkable potential for electronics.



INTRODUCTION

The rapid development of wearable yet intelligent electronics defines an urgent need of innovation in miniaturization, flexibility, and integration of microscale energy storage devices.^{1–4} Lithium microbatteries are commercially important microscale power sources but represent limited cycle life, low power density, poor low-temperature kinetics, and lithium-related safety issues. Further, such microbatteries suffer from limited miniaturization and are not well compatible with integrated circuits.^{5–7} Recently, planar microsupercapacitors (MSCs), characterized by ultrahigh power density, long-term cyclability, robust flexibility, and high safety, appear as competitive alternatives to complement or replace microbatteries for on-chip energy storage.^{8–10} So far, notable efforts have been made toward high pseudocapacitive electrodes of metal oxides (e.g., RuO_2 ,¹¹ MnO_2 ,¹² $\text{Ni}(\text{OH})_2$,¹³ CoO ¹⁴) and conducting polymers (polyaniline,¹⁵ polypyrrole¹⁶) for MSCs,

but these MSCs still represent unsatisfying power capability and cyclability.^{17,18} To this end, nanoporous carbon,¹⁹ carbide-derived carbon,⁹ onion-like carbon,²⁰ carbon nanotubes (CNTs),²¹ and graphene^{22–27} have emerged as the most appealing candidates for high-power and long-life MSCs.

Recently, graphene-based MSCs, including reduced graphene oxide,^{22–27} graphene quantum dots,²⁸ graphene/CNTs,^{29,30} graphene/polyaniline,³¹ graphene/thiophene,³² graphene/ MnO_2 ,³³ and graphene/phosphorene,³⁴ have been intensively exploited. These MSCs can completely combine the advantages of the planar device configuration and the unique features of graphene (e.g., 2D thickness, flexibility) for maximizing charge storage^{23,25,26} and thus furnish thinner, smaller, and more flexible devices.^{35,36} To boost volumetric

Received: March 28, 2018

Published: June 12, 2018

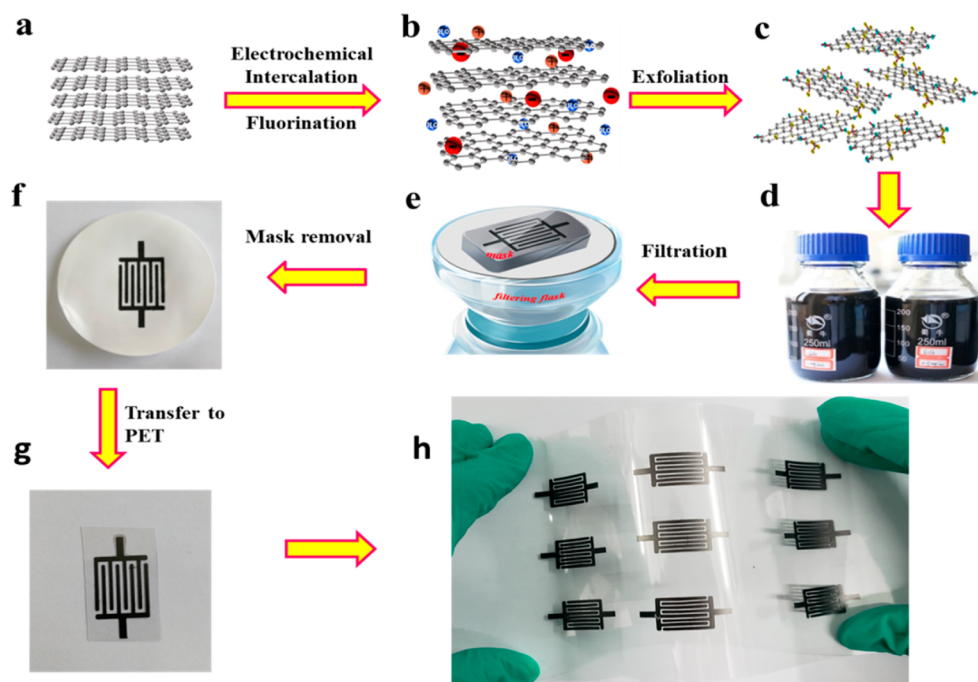


Figure 1. Schematic of the fabrication of FG-MSCs. (a–c) Illustration of electrochemical exfoliation of graphite to FG nanosheets in 0.1 M NaBF₄ aqueous electrolyte, via intercalation, fluorination, and exfoliation (red balls: BF₄[−] anion; blue balls: H₂O molecule). (d) Photograph of as-prepared FG ink, 0.5 mg mL^{−1} in water. (e) Fabrication of FG patterns with mask-assisted filtration. (f) Photograph of the as-fabricated FG electrodes on the PTFE membrane. (g) Transfer of FG electrodes onto the PET substrate. (h) Photograph of nine FG-MSCs obtained on a flexible PET substrate.

performance of MSCs, incorporation with single or dual heteroatoms (e.g., N,³⁷ B,³⁸ S³⁹) into graphene lattices is a versatile protocol due to additional pseudocapacitive effects. In particular, introduction of fluorine (F), possessing excessive high electronegativity, may be promising for optimizing electrical properties of graphene. Indeed, this concept yields better electrochemical performance because of the synergistic effects of increasing disorder and defects which expand interlayer spacing and produce novel active sites of semi-ionic C–F bonds.^{40,41} On the other hand, high-voltage MSCs using ionogel electrolyte, a gel-like form of ionic liquid with solid component (e.g., polymer, silica), are arising as a novel class of microscale power source. This is because they can overcome the critical issues of the operating voltage barely exceeding 1 V of aqueous hydrogel polymer electrolytes and the leakage of liquid electrolytes. Despite the great success of chemically modified graphene (N,³⁷ B,³⁸ S³⁹) for MSCs, scalable production of fluorine-functionalized graphene for high-energy ionogel-based MSCs has not yet been reported.

Here we describe a scalable, single-step electrochemical exfoliation of graphite into highly solution-processable fluorine-modified graphene (FG) for flexible and high-performance ionogel-based MSCs (denoted as FG-MSCs) with high volumetric energy density. Electrochemical exfoliation and fluorine incorporation of graphene nanosheets are simultaneously achieved by intercalation and fluorination with fluorine-containing inorganic salts under neutral and mild conditions. Notably, FG nanosheets show atomically thin, large lateral size of up to 12 μm, high yield of >70% with ≤3 layers, and uniform fluorine incorporation of 3 at%. Moreover, such exfoliated FG nanosheets are readily used to produce highly solution-processable ink (1 mg mL^{−1}) in water without the use of any surfactants, allowing for scalable production of large-area FG films. Furthermore, the as-fabricated FG-MSCs, using

ionogel-based electrolyte of 1-ethyl-3-methylimidazolium tetrafluoroborate with poly(vinylidene fluoride-hexafluoropropylene) (EMIMBF₄/PVDF-HFP), can work at a high voltage of 3.5 V. Remarkably, our microdevices deliver high volumetric energy density of 56 mWh cm^{−3}, outperforming the most reported MSCs up to date. Meanwhile, FG-MSCs exhibit outstanding flexibility with ~100% of initial capacitance even at a high bending angle of 180° and efficient parallel and serial integration for enhancing the capacitance and voltage output.

RESULTS AND DISCUSSION

Fabrication of FG Nanosheets and FG-MSCs. The fabrication of FG-MSCs is schematically illustrated in Figure 1. First, FG nanosheets were readily generated in a two-electrode system, using platinum foil as counter electrode and graphite as working electrode, in fluorine-containing neutral electrolytes, e.g., NaBF₄, NH₄BF₄, and KPF₆. The exfoliation and fluorination process of FG nanosheets occurred simultaneously (Figure 1a–c, for example, in NaBF₄ electrolyte) and involved the following steps: (i) Applying a bias voltage allows for the reduction of water, creating the strongly nucleophilic hydroxyl ions (OH[−]), and thus attacking the edges of graphite initially.^{42,43} (ii) Subsequent oxidation with OH[−] and synchronous fluorination with BF₄[−] at the edges accelerate the depolarization and expansion of graphitic layers, thereby facilitating the intercalation of BF₄[−] into the interior of interlayer spacing. (iii) Continuous oxidation of BF₄[−] anions and water produce gaseous species such as O₂, all of which provide large forces to separate weakly bonded graphitic layers (Figure 1c). The stable ink of FG nanosheets, collected after filtration and washing, was obtained via sonication (Figure 1d). In comparison with the conventional Hummers method and chemical vapor deposition that usually involve a time-consuming laborious procedure, high temperature, multistep

processes, and aggressive reagents, our electrochemical exfoliation protocol is a fast, straightforward yet scalable approach for mass production of gram-scale FG nanosheets at the laboratory (~ 1.8 g in a 250 mL beaker, Figure 2a,b), suggesting the industrial applicability.^{42,43}

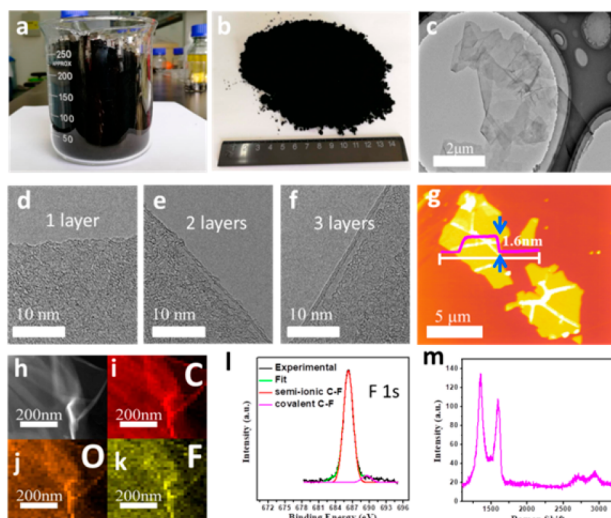


Figure 2. Morphological and structural characterization of FG nanosheets, exfoliated in 0.1 M NaBF₄ aqueous electrolyte. (a, b) FG powder on a gram scale (~ 1.8 g in 250 mL beaker), indicative of the scalability of our approach. (c) TEM image of FG nanosheets. (d–f) HRTEM images of (d) single-layer, (e) double-layer, and (f) three-layer FG nanosheets. (g) AFM image (inset: height profile of FG nanosheets). (h) Scanning transmission electron microscopy (STEM) image and (i) carbon, (j) oxygen, and (k) fluorine element mapping images of a FG nanosheet taken in (h). (l) F 1s XPS spectrum of FG nanosheets. (m) Raman spectrum of FG nanosheets.

Scanning electron microscopy (SEM, Figures S1 and S2) displayed uniform features over large area and flat sheet-like morphology, revealing 88% of FG nanosheets with lateral sizes of 3–12 μm (Figure S3). Transmission electron microscopy (TEM, Figure 2c, Figure S4) showed transparent and ultrathin FG nanosheets, with a predominant number of ≤ 3 layers, in a high yield of 70% due to statistical analysis (Figure S5). Atomic force microscopy (AFM, Figure 2g) measurements underscored the uniform thickness of 1.6 nm, corresponding to 2 layers of typical FG nanosheets. The homogeneous fluorine incorporation of FG nanosheets was unraveled by the elemental mapping images of carbon, oxygen, and fluorine (Figure 2h–k). The existence of fluorine was also confirmed by X-ray photoelectron spectroscopy (XPS, Figure 2l), showing a major F 1s peak of semi-ionic C–F bonds at 686.2 eV, corresponding to the isolated fluorine centers attached to the graphene basal plane, and a weak broad peak at 689.5 eV of covalent C–F bonds.^{40,41} Further, XPS analysis represented the contents of approximately 3 at% fluorine and 19 at% oxygen appearing in FG nanosheets (Table S1). The Raman spectrum of FG reveals a strong D band at 1352 cm^{-1} and G band at 1604 cm^{-1} (Figure 2m) and has a larger I_D/I_G ratio of ~ 1.25 than that of undoped electrochemically exfoliated graphene (EG, 0.1–0.3),^{42,43} due to the induced dissymmetry of fluorine functionalization. The X-ray diffraction pattern of FG nanosheets (Figure S6) revealed an expanded interlayer d -spacing of 3.48 Å in comparison with graphite (3.36 Å), indicative of F modification in graphene.

Unlike FG nanosheets prepared by previous fluorination of graphene oxide, this is the first demonstration of electrochemically exfoliated graphene functionalized with fluorine.

The FG patterned electrodes for MSCs were directly manufactured through mask-assisted filtration of the resulting FG ink (0.5 mg mL^{-1}) (Figure 1d,e). Then, the interdigitated patterns of FG films on the polytetrafluoroethylene (PTFE, Figure 1f) membrane were readily dry-transferred onto a flexible polyethylene terephthalate (PET) substrate (Figure 1g), directly acting as binder- and additive-free electrodes (Figure S7 and S8), without the need of metal-based current collectors. Finally, after drop casting of ionic liquid electrolytes (e.g., EMIMBF₄, EMIMBF₄/PVDF-HFP) and device package, FG-MSCs were produced. It is worth noting that our developed strategy is highly robust for facile production of FG-MSCs arrays on flexible substrates (Figure 1h).

Electrochemical Performance of Liquid-Based FG-MSCs. The electrochemical performance of FG-MSCs was first examined at a voltage of 3.5 V in liquid electrolyte of EMIMBF₄ by cyclic voltammetry (CV) curves (Figure 3a, Figure S9) and galvanostatic charge and discharge (GCD) profiles (Figure S10). To highlight the importance of fluorine attachment, we also fabricated two MSCs, one based on

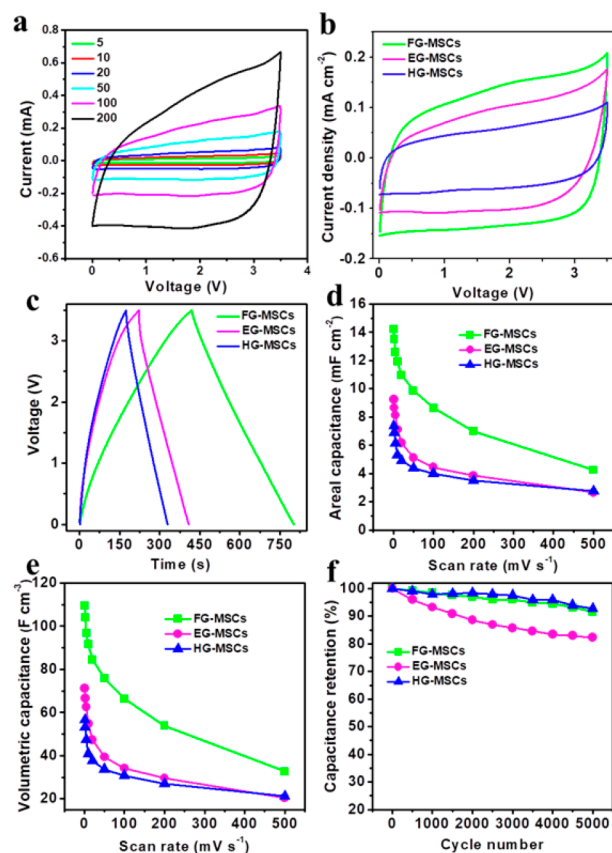


Figure 3. Electrochemical characterization of FG-MSCs in liquid electrolyte of EMIMBF₄. (a) CVs of FG-MSCs obtained at different scan rates of 5–200 mV s^{-1} . (b) CVs measured at scan rate of 50 mV s^{-1} and (c) GCDs tested at current density of 0.2 A cm^{-2} of FG-MSCs, EG-MSCs, and HG-MSCs. (d) Areal capacitance and (e) volumetric capacitance of FG-MSCs, EG-MSCs, and HG-MSCs as a function of scan rate. (f) Cycling stability of FG-MSCs, EG-MSCs, and HG-MSCs for 5000 cycles obtained at a current density of 0.2 A cm^{-2} .

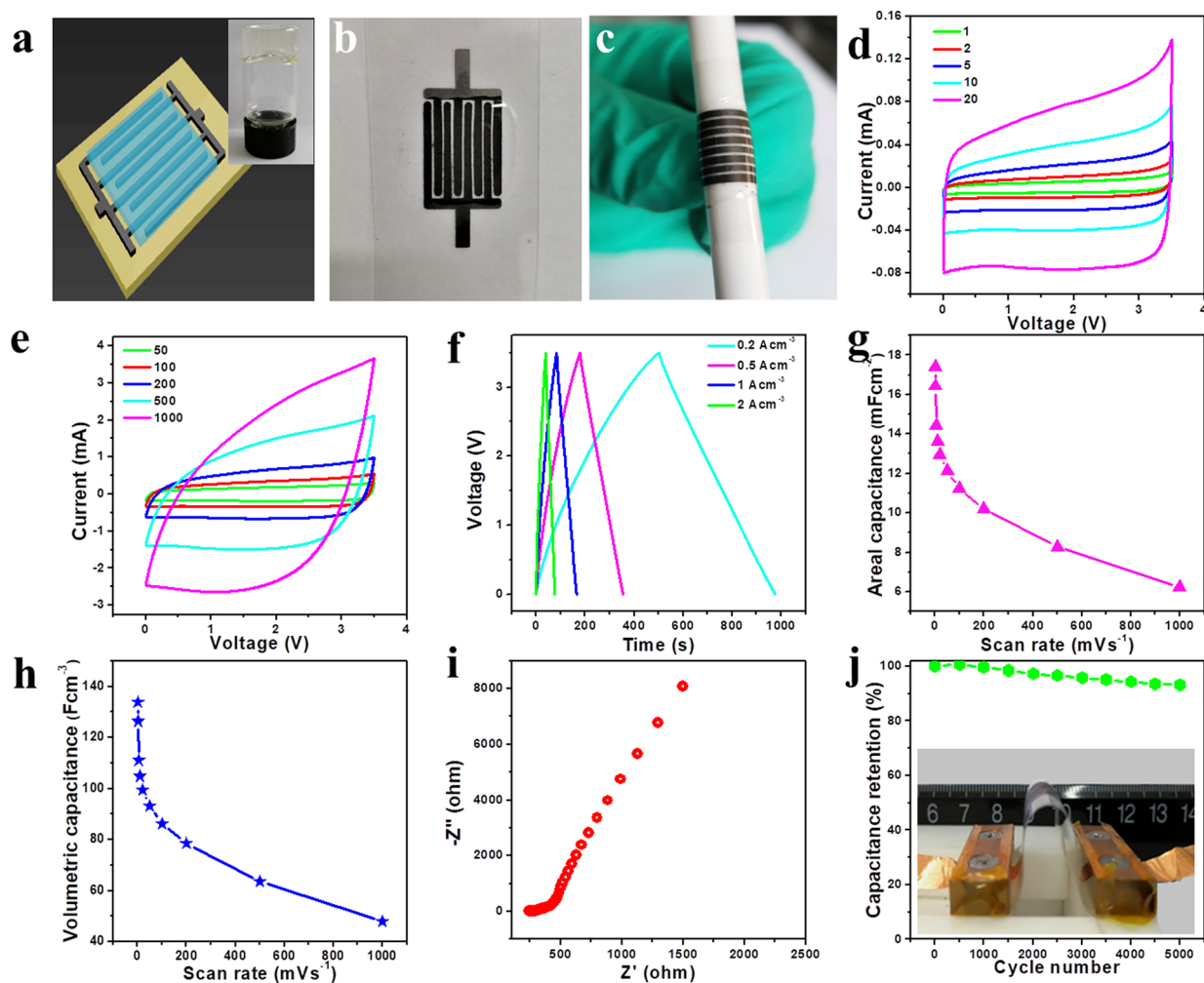


Figure 4. Fabrication and electrochemical characterization of ionogel-based FG-MSCs. (a) Schematic (inset: EMIMBF₄/PVDF-HFP ionogel electrolyte) and (b, c) photographs of FG-MSCs using ionogel electrolyte of EMIMBF₄/PVDF-HFP. (d, e) CVs obtained at varying scan rates of (d) 1–20 mV s⁻¹ and (e) 50–1000 mV s⁻¹. (f) GCD profiles tested at different current densities of 0.2–2 A cm⁻². (g) Areal capacitance and (h) volumetric capacitance of ionogel-based FG-MSCs. (i) EIS and (j) cycling stability of ionogel-based FG-MSCs under constant bending state (inset: bending FG-MSCs).

undoped electrochemically EG (10 at% oxygen) prepared in 0.2 M H₂SO₄ (EG-MSCs)⁴⁴ and another based on hydrothermally treated FG (HG, 13 at% oxygen and 0.6 at% fluorine, Table S1) (HG-MSCs), while the film formation process and cell assembly were kept the same as FG-MSCs. The CVs of FG-MSCs presented a pronounced capacitive behavior with nearly symmetric rectangular shape at low scan rates of 1–20 mV s⁻¹ and displayed a trapezoid shape at high rates of 50–200 mV s⁻¹, likely associated with the structural changes throughout the loading process caused by large ions of EMIMBF₄ (Figure 3a, Figure S9). The excellent electrochemical properties of FG-MSCs were also confirmed by GCD profiles with negligible IR voltage drop even at high current densities (Figure S10). FG-MSCs displayed much higher areal current density (Figure 3b) and longer discharge time (Figure 3c) than those of EG-MSCs and HG-MSCs, indicative of fluorine functionalization greatly enhancing the capacitance. Areal capacitance and volumetric capacitance of FG-MSCs, EG-MSCs, and HG-MSCs are compared in Figure 3d and 3e, respectively. Apparently, FG-MSCs delivered an exceptional areal capacitance of 14.2 mF cm⁻² and volumetric capacitance of 110 F cm⁻³ at 1 mV s⁻¹, both of which were much higher

than those of EG-MSCs (9.3 mF cm⁻² and 70 F cm⁻³ at 1 mV s⁻¹) and HG-MSCs (7.4 mF cm⁻² and 57 F cm⁻³ at 1 mV s⁻¹). Moreover, high capacitances of 4.3 mF cm⁻² and 33 F cm⁻³ were still attained at a large scan rate of 500 mV s⁻¹. In sharp contrast, low capacitances of 2.7 mF cm⁻² and 21.4 F cm⁻³ for EG-MSCs and 2.5 mF cm⁻² and 20 F cm⁻³ for HG-MSCs were obtained at a scan rate of 500 mV s⁻¹. Similarly, the performance improvement of FG-MSCs was also evidenced by GCD measurements (Figure 3c). Moreover, electrochemical impedance spectra (EIS) measurements elucidated the better capacitive behavior of FG-MSCs, with a larger slope, than the other two MSCs (Figure S11) at low frequency, manifesting the fast ionic diffusion of FG-MSCs. FG-MSCs and HG-MSCs displayed outstanding cycling stability, with a larger capacitance retention of 91% than that of EG-MSCs (82%) after 5000 cycles (Figure 3f). This result suggests that FG films featuring highly electrical conductivity (520 S cm⁻¹) and excellent interfacial wettability (a low contact angle of 25.8° against EMIMBF₄, Figure S12) could allow both rapid electron transfer and ion diffusion from electrolyte to electrode. In addition, with increasing film thickness, FG-MSCs displayed an increased areal capacitance from 8.1 to 24 mF cm⁻² and slowly

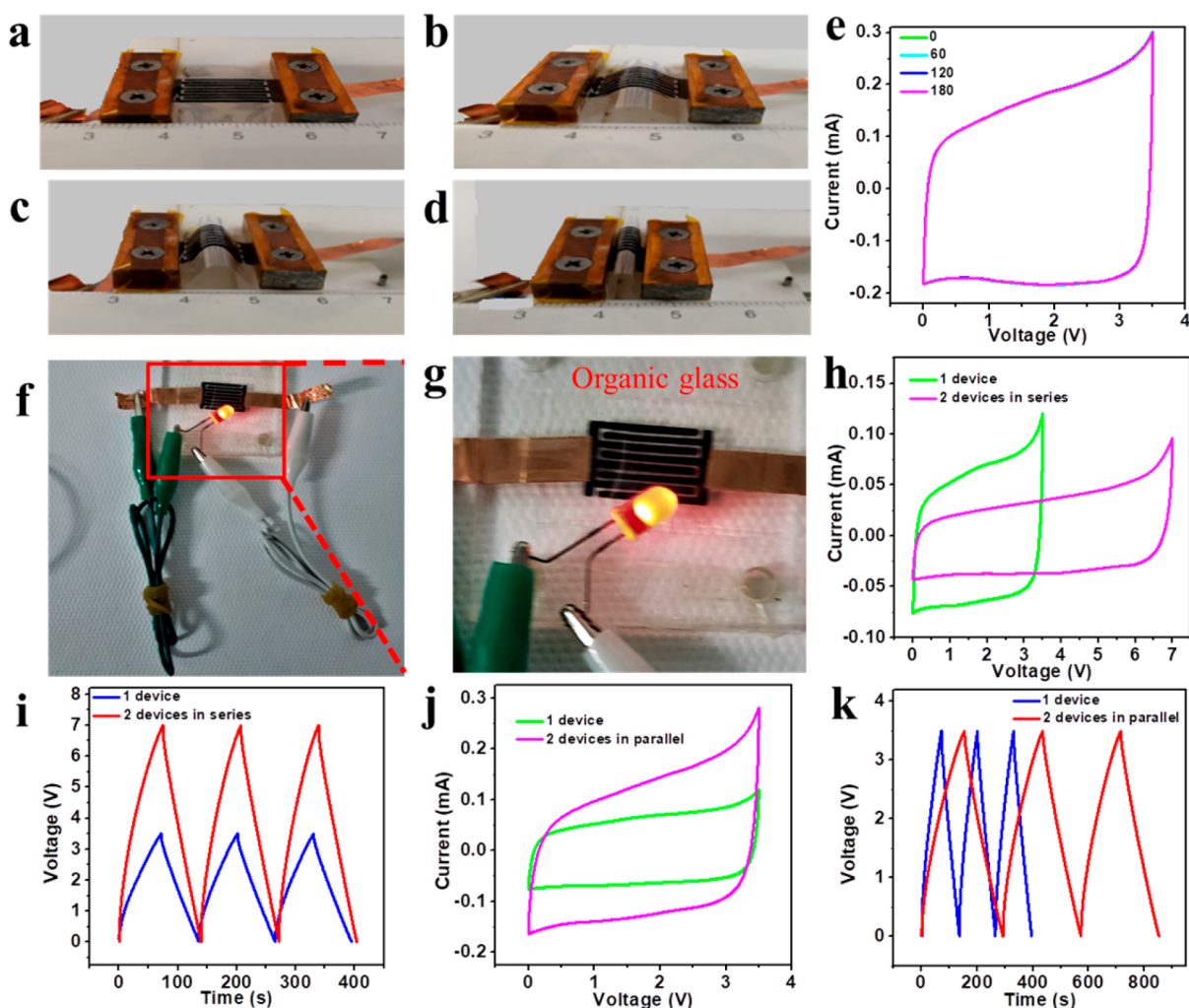


Figure 5. Superior flexibility and integration of ionogel-based FG-MSCs. (a–d) Photographs and (e) CVs of ionogel-based FG-MSCs under various bending angles of (a) 0, (b) 60, (c) 120, and (d) 180°. (f, g) Photographs of FG-MSCs (placed on the organic glass) after charging to 3.5 V at 0.5 A cm^{-2} to power a LED light. (h) CV curves tested at 50 mV s^{-1} and (i) GCD profiles measured at 1 A cm^{-2} of two FG-MSCs connected in series. (j) CV curves obtained at 50 mV s^{-1} and (k) GCD profiles tested at 1 A cm^{-2} of two FG-MSCs connected in parallel.

declined volumetric capacitance from 115 to 92 F cm^{-3} (Figure S13). This can be explained by the reduced slopes of EIS at low frequency with increasing film thickness (Figure S14), manifesting the low ionic diffusion in thicker film.

Ionogel-Based FG-MSCs. Flexible and portable electronics always require their appropriate microscale power sources, e.g., supercapacitors, which are highly flexible and give high voltage output and large energy and power densities. Unlike aqueous hydrogel polymer electrolytes with low operation voltage $\leq 1 \text{ V}$, ionogel-based MSCs are promising for all-solid-state high-voltage MSCs that preserve several intriguing properties, e.g. wide electrochemical window, excellent thermal stability, and nonvolatility of ionic liquid, enabling facile shaping and flexible operation of the cell without involving the leakage of liquid electrolytes. To this end, we further constructed all-solid-state ionogel-based FG-MSCs, using EMIMBF₄/PVDF-HFP electrolyte (Figure 4a–c). The CV curves were tested at varying scan rates of 1 – 1000 mV s^{-1} (Figure 4d,e), and GCD profiles were measured at different current densities of 0.2 – 2 mA cm^{-2} , as shown in Figure 4f. The almost ideal CV curves and triangular charge and discharge profiles at varying scan rates demonstrated outstanding capacitive behavior. Remarkably, our device can be

operated well at a large voltage of 3.5 V and deliver ultrahigh charge and discharge rates (up to 1000 mV s^{-1}), well comparable to those with liquid electrolyte of EMIMBF₄ (Figure 3). Interestingly, ionogel-based FG-MSCs offered high areal capacitance of 17.4 mF cm^{-2} (Figure 4g) and volumetric capacitance of 134 F cm^{-3} (Figure 4h) at 1 mV s^{-1} , much higher than those with liquid EMIMBF₄ (14.2 mF cm^{-2} and 109 F cm^{-3} at 1 mV s^{-1} , Figure 3d,e). Furthermore, both of them were much higher than those of the most reported carbon-based MSCs, such as 0.32 mF cm^{-2} and 71.6 F cm^{-3} for methane plasma reduced graphene oxide (rGO),²³ 0.28 mF cm^{-2} and 0.76 F cm^{-3} for vertically aligned CNTs,²¹ 2 mF cm^{-2} and 29.4 F cm^{-3} for laser written GO film,²² 9.9 mF cm^{-2} and 7.6 F cm^{-3} for onion-like carbon,²⁰ 40 mF cm^{-2} and 29.4 F cm^{-3} for rGO/CNTs,²⁹ and 14.7 mF cm^{-2} and 19 F cm^{-3} for laser-scribed graphene,²⁴ respectively (Table S2). When operated even at a high rate of 100 mV s^{-1} , the capacitance of ionogel-based FG-MSCs declines only slightly to 11 mF cm^{-2} and 99 F cm^{-3} (Figure 4g,h), still higher than those of liquid-based devices (8.7 mF cm^{-2} and 78 F cm^{-3} , Figure 3d, e). The anomalous performance enhancement is mainly attributed to the higher ionic conductivity of EMIMBF₄-based ionogel electrolyte (25 mS cm^{-1}) with the optimal content of PVDF-

HFP (10 wt%) than that of liquid EMIMBF₄ (13.8 mS cm⁻¹) (Figure 4i, Figure S15).⁴⁵ Moreover, our ionogel-based FG-MSCs exhibited exceptional cycling stability, with a remarkable capacitance retention of 93% after 5000 cycles (Figure 4j).

Flexibility and Integration of FG-MSCs. To demonstrate the robust flexibility of as-fabricated microdevices, we further examined the CVs of ionogel-based FG-MSCs under various bending angles of 0, 60, 120, and 180° (Figure 5a–d). It is disclosed that CV curves with different bending angles changed slightly, and almost 100% of initial capacitance was kept when even bended at 180° (Figure 5e), demonstrating an outstanding mechanical flexibility. More importantly, the single cell can efficiently combine high voltage output and high storage capability. For instance, the single microdevice, after charging to 3.5 V with 0.5 A cm⁻², could readily power a light-emitting diode (LED) for a significant time of more than 60 s (Figure 5f,g). Moreover, FG-MSCs could be easily connected in series and parallel, without any metal-based interconnects and contacts, to efficiently boost the operating voltage and capacitance output in ionogel electrolyte (Figure 5h–k). For instance, the CV and GCD profiles presented a sufficient voltage extension from 3.5 V for a single cell to 7.0 V for two tandem cells (Figure 5h,i). Meanwhile, double capacitance enhancement was apparently attained from two parallelly connected FG-MSCs in comparison with a single cell (Figure 5j,k), suggesting superior modular integration.

Figure 6 shows the Ragone plot of our FG-MSCs in different electrolytes compared with commercially available energy

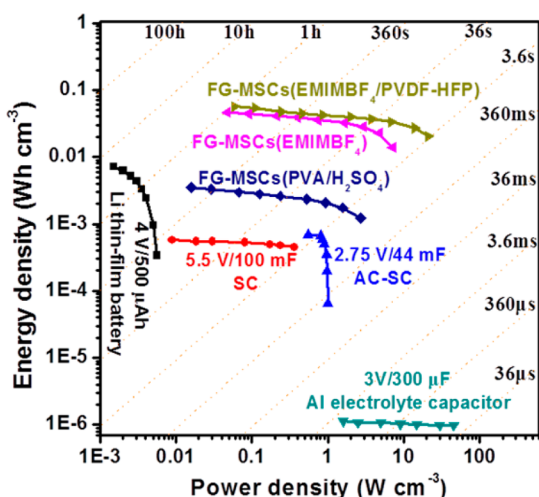


Figure 6. Ragone plot of FG-MSCs in different electrolytes in comparison with lithium thin-film battery (4 V/500 μ Ah), electrolytic capacitor (3 V/300 μ F), and activated carbon supercapacitors (AC-SC, 2.75 V/44 mF).

storage devices. Notably, the ionogel-based FG-MSCs delivered high volumetric energy density of 56 mWh cm⁻³, which is much higher than those measured in other electrolytes, e.g., 46 mWh cm⁻³ in EMIMBF₄ and 3.5 mWh cm⁻³ in poly(vinyl alcohol) (PVA)/H₂SO₄ (Figure S16), and 1 order of magnitude higher than those of most reported MSCs, such as 2.1 mWh cm⁻³ for laser-scribed graphene,²⁴ 2.5 mWh cm⁻³ for methane plasma rGO,²³ 2.3 mWh cm⁻³ for inkjet-printed carbon,⁴⁶ 3.2 mWh cm⁻³ for carbide-derived carbon,⁸ 0.3 mWh cm⁻³ for vertically aligned CNTs,²¹ 1.6 mWh cm⁻³ for onion-like carbon,²⁰ and lithium thin-film batteries (\leq 10

mWh cm⁻³). Moreover, our FG-MSCs offered a power density of \sim 21 W cm⁻³, much comparable to electrolytic capacitors. Therefore, our FG-MSCs possess great potential as a high-voltage and high-energy microscale power source for flexible electronics that require high operating voltage and energy in a short time frame.

The excellent electrochemical performance of ionogel-based FG-MSCs is attributed to the elaborated screening and synergetic integration of each isolated device component into one single cell. First, electrochemically exfoliated FG nanosheets are atomically thin and feature large lateral size, uniform fluorine doping, and high solution processability. These advantages allow the efficient formation of highly conductive (520 S cm⁻¹), flexible, and compact FG patterns, engineered by a mask-assisted approach, without the need of any metal-based current collectors. Second, the utilization of EMIMBF₄/PVDF-HFP ionogels, characteristic of high ionic conductivity (25 mS cm⁻¹), can not only advance the manufacturing of all-solid-state high-voltage and flexible MSCs but also maintain the strong interfacial wettability between electrolyte and electrode. Third, fluorine incorporation creates many electrochemically active sites (e.g., semi-ionic C–F bonds) and thus provides additional pseudocapitance. Finally, ultrathin and flexible 2D nanosheets in planar FG-MSCs with extremely short ionic pathways can abundantly form parallel ion channels for fast ion adsorption and surface redox reaction, thus offering high rate capability and maximal energy storage.

CONCLUSION

In summary, we have developed a single-step electrochemical protocol to generate high-quality FG nanosheets for flexible and on-chip ionogel-based MSCs with high volumetric energy density, outstanding flexibility, exceptional cyclability, high voltage output, and superior integration. Our approach is highly scalable for the environmentally friendly gram production of solution-processable FG nanosheets using neutral aqueous electrolytes and facile for the creation of high-voltage and high-energy MSCs. Therefore, our strategy will pave the way for scalable and fast exfoliation of graphite to chemically modified graphene and for large-scale production of flexible and high-energy ionogel-based MSC arrays that satisfy the stringent requirement of wearable electronics.

EXPERIMENTAL SECTION

Electrochemical Production of FG Nanosheets. Typically, graphite foil (0.13 mm, carbon content: 99.8%, Alfa Aesar) was chosen as working electrode, and a Pt foil was used as counter electrode, both of which were immersed in 0.1 M NaBF₄ aqueous electrolytes. The distance between graphite and Pt foil was \sim 2 cm. Electrochemical exfoliation of graphite was conducted by applying positive voltage at 10 V for 15 min. Afterward, the exfoliated product was collected on a PTFE membrane (pore size 0.2 μ m) by filtration and washed several times with deionized water. The resultant product was dispersed in water by sonication for 40 min and let to stand for 24 h at room temperature. Finally, the supernatant of FG nanosheets was used for characterization and thin-film fabrication.

Preparation of Ionogel Electrolyte. PVDF-HFP polymer was fully dissolved in acetone. Then, EMIMBF₄, dried in a vacuum oven at 105 °C for 5 h, was mixed with the above solution of PVDF-HFP/acetone and stirred magnetically for 1 h. The optimal mass ratio of EMIMBF₄ and PVDF-HFP was adjusted to be \sim 9. The resultant ionogel electrolyte of EMIMBF₄/PVDF-HFP was slowly drop-casted on the project area of electrode patterns.

Materials Characterization. The morphology and structure of graphene nanosheets and as-fabricated films were examined using

SEM (JSM-7800F), TEM (JEM-2100), AFM (Cypher ES, Oxford instrument), XPS (ESCALAB 250 instrument equipped with a nonmonochromatic Mg-Ka X-ray source), XRD (X'pert Pro), and Raman spectrometry (LabRAM HR800). The electrical conductivity of film electrodes was examined by a standard four-point probe system (RTS-9). Thickness, 2D pseudocolor view, and 3D view of the surface of the FG electrode on PET substrate were measured using a stylus profiler (Alpha step D-600, KLA-Tencor, USA).

Electrochemical Measurement. The electrochemical performances were performed by an electrochemical workstation (CHI760E), using CV measurements at different scan rates from 1 to 1000 mV s⁻¹, GCD profiles at different current densities, and EIS recorded in the frequency range from 0.01 Hz to 100 kHz with ac amplitude of 5 mV.

■ ASSOCIATED CONTENT

Supporting Information

The Supporting Information is available free of charge on the ACS Publications website at DOI: 10.1021/jacs.8b03235.

Calculation of areal/volumetric capacitance, power/energy density, TEM, SEM, AFM, and EDX analysis characterization of SG film, CVs of SG-MSCs, and Tables S1 and S2 (PDF)

■ AUTHOR INFORMATION

Corresponding Authors

*xinliang.feng@tu-dresden.de

*muellen@mpip-mainz.mpg.de

*wuzs@dicp.ac.cn

ORCID

Qiang Fu: 0000-0001-5316-6758

Xinhe Bao: 0000-0001-9404-6429

Xinliang Feng: 0000-0003-3885-2703

Klaus Müllen: 0000-0001-6630-8786

Zhong-Shuai Wu: 0000-0003-1851-4803

Notes

The authors declare no competing financial interest.

■ ACKNOWLEDGMENTS

This work was financially supported by the National Natural Science Foundation of China (Grant 51572259), National Key R&D Program of China (Grants 2016YFB0100100, 2016YFA0200200), Recruitment Program of Global Expert (1000 Talent Plan), Natural Science Foundation of Liaoning Province (Grant 201602737), DICP (DICP ZZBS201708, DICP MTO201502), DICP&QIBEBT (Grant DICP&QIBEBT UN201702), Dalian National Laboratory For Clean Energy (DNL), CAS, Exploratory Research Program of Shaanxi Yanchang Petroleum (Group) Co., LTD & DICP, and Datong Coal Mine Group Co., Ltd.

■ REFERENCES

- (1) LeMieux, M. C.; Bao, Z. *Nat. Nanotechnol.* **2008**, *3*, 585.
- (2) Gates, B. D. *Science* **2009**, *323*, 1566.
- (3) Yu, D.; Goh, K.; Wang, H.; Wei, L.; Jiang, W.; Zhang, Q.; Dai, L.; Chen, Y. *Nat. Nanotechnol.* **2014**, *9*, 555.
- (4) Liu, C.; Li, F.; Ma, L. P.; Cheng, H. M. *Adv. Mater.* **2010**, *22*, E28.
- (5) Wan, S.; Peng, J.; Jiang, L.; Cheng, Q. *Adv. Mater.* **2016**, *28*, 7862.
- (6) Wang, X.; Lu, X.; Liu, B.; Chen, D.; Tong, Y.; Shen, G. *Adv. Mater.* **2014**, *26*, 4763.
- (7) Wen, L.; Li, F.; Cheng, H.-M. *Adv. Mater.* **2016**, *28*, 4306.
- (8) Beidaghi, M.; Gogotsi, Y. *Energy Environ. Sci.* **2014**, *7*, 867.

(9) Chmiola, J.; Largeot, C.; Taberna, P.-L.; Simon, P.; Gogotsi, Y. *Science* **2010**, *328*, 480.

(10) Huang, P.; Lethien, C.; Pinaud, S.; Brousse, K.; Laloo, R.; Turq, V.; Respaud, M.; Demortiere, A.; Daffos, B.; Taberna, P. L.; Chaudret, B.; Gogotsi, Y.; Simon, P. *Science* **2016**, *351*, 691.

(11) Ferris, A.; Garbarino, S.; Guay, D.; Pech, D. *Adv. Mater.* **2015**, *27*, 6625.

(12) Su, Z.; Yang, C.; Xie, B.; Lin, Z.; Zhang, Z.; Liu, J.; Li, B.; Kang, F.; Wong, C. P. *Energy Environ. Sci.* **2014**, *7*, 2652.

(13) Kurra, N.; Alhebshi, N. A.; Alshareef, H. N. *Adv. Energy Mater.* **2015**, *5*, 1401303.

(14) Zhu, Y. G.; Wang, Y.; Shi, Y.; Wong, J. I.; Yang, H. Y. *Nano Energy* **2014**, *3*, 46.

(15) Wang, K.; Zou, W.; Quan, B.; Yu, A.; Wu, H.; Jiang, P.; Wei, Z. *Adv. Energy Mater.* **2011**, *1*, 1068.

(16) Liu, S.; Gordichuk, P.; Wu, Z.-S.; Liu, Z.; Wei, W.; Wagner, M.; Mohamed-Noriega, N.; Wu, D.; Mai, Y.; Herrmann, A.; Müllen, K.; Feng, X. *Nat. Commun.* **2015**, *6*, 8817.

(17) Zhai, Y.; Dou, Y.; Zhao, D.; Fulvio, P. F.; Mayes, R. T.; Dai, S. *Adv. Mater.* **2011**, *23*, 4828.

(18) Kurra, N.; Ahmed, B.; Gogotsi, Y.; Alshareef, H. N. *Adv. Energy Mater.* **2016**, *6*, 1601372.

(19) Wei, L.; Nitta, N.; Yushin, G. *ACS Nano* **2013**, *7*, 6498.

(20) Pech, D.; Brunet, M.; Durou, H.; Huang, P.; Mochalin, V.; Gogotsi, Y.; Taberna, P.-L.; Simon, P. *Nat. Nanotechnol.* **2010**, *5*, 651.

(21) Ghosh, A.; Viet Thong, L.; Bae, J. J.; Lee, Y. H. *Sci. Rep.* **2013**, *3*, 2939.

(22) Liu, Z.; Wu, Z.-S.; Yang, S.; Dong, R.; Feng, X.; Müllen, K. *Adv. Mater.* **2016**, *28*, 2217.

(23) Niu, Z.; Zhang, L.; Liu, L.; Zhu, B.; Dong, H.; Chen, X. *Adv. Mater.* **2013**, *25*, 4035.

(24) Wu, Z.-K.; Lin, Z.; Li, L.; Song, B.; Moon, K.-s.; Bai, S.-L.; Wong, C.-P. *Nano Energy* **2014**, *10*, 222.

(25) El-Kady, M. F.; Kaner, R. B. *Nat. Commun.* **2013**, *4*, 1475.

(26) Wu, Z.-S.; Parvez, K.; Feng, X.; Müllen, K. *Nat. Commun.* **2013**, *4*, 2487.

(27) Gao, W.; Singh, N.; Song, L.; Liu, Z.; Reddy, A. L. M.; Ci, L.; Vajtai, R.; Zhang, Q.; Wei, B.; Ajayan, P. M. *Nat. Nanotechnol.* **2011**, *6*, 496.

(28) Liu, W.-W.; Feng, Y.-Q.; Yan, X.-B.; Chen, J.-T.; Xue, Q.-J. *Adv. Funct. Mater.* **2013**, *23*, 4111.

(29) Beidaghi, M.; Wang, C. *Adv. Funct. Mater.* **2012**, *22*, 4501.

(30) Lin, J.; Zhang, C.; Yan, Z.; Zhu, Y.; Peng, Z.; Hauge, R. H.; Natelson, D.; Tour, J. M. *Nano Lett.* **2013**, *13*, 72.

(31) Wu, Z. S.; Parvez, K.; Li, S.; Yang, S.; Liu, Z. Y.; Liu, S. H.; Feng, X. L.; Müllen, K. *Adv. Mater.* **2015**, *27*, 4054.

(32) Wu, Z.-S.; Zheng, Y.; Zheng, S.; Wang, S.; Sun, C.; Parvez, K.; Ikeda, T.; Bao, X.; Müllen, K.; Feng, X. *Adv. Mater.* **2017**, *29*, 1602960.

(33) Peng, L.; Peng, X.; Liu, B.; Wu, C.; Xie, Y.; Yu, G. *Nano Lett.* **2013**, *13*, 2151.

(34) Xiao, H.; Wu, Z.-S.; Chen, L.; Zhou, F.; Zheng, S.; Ren, W.; Cheng, H.-M.; Bao, X. *ACS Nano* **2017**, *11*, 7284.

(35) Heon, M.; Lofland, S.; Applegate, J.; Nolte, R.; Cortes, E.; Hettlinger, J. D.; Taberna, P.-L.; Simon, P.; Huang, P.; Brunet, M.; Gogotsi, Y. *Energy Environ. Sci.* **2011**, *4*, 135.

(36) Lukatskaya, M. R.; Mashtalir, O.; Ren, C. E.; Dall'Agnese, Y.; Rozier, P.; Taberna, P. L.; Naguib, M.; Simon, P.; Barsoum, M. W.; Gogotsi, Y. *Science* **2013**, *341*, 1502.

(37) Wu, Z.-S.; Parvez, K.; Winter, A.; Vieker, H.; Liu, X.; Han, S.; Turchanin, A.; Feng, X.; Müllen, K. *Adv. Mater.* **2014**, *26*, 4552.

(38) Peng, Z.; Ye, R.; Mann, J. A.; Zakhidov, D.; Li, Y.; Smalley, P. R.; Lin, J.; Tour, J. M. *ACS Nano* **2015**, *9*, 5868.

(39) Wu, Z.-S.; Tan, Y.-Z.; Zheng, S.; Wang, S.; Parvez, K.; Qin, J.; Shi, X.; Sun, C.; Bao, X.; Feng, X.; Müllen, K. *J. Am. Chem. Soc.* **2017**, *139*, 4506.

(40) Huang, S.; Li, Y.; Feng, Y.; An, H.; Long, P.; Qin, C.; Feng, W. *J. Mater. Chem. A* **2015**, *3*, 23095.

- (41) Zhou, J.; Lian, J.; Hou, L.; Zhang, J.; Gou, H.; Xia, M.; Zhao, Y.; Strobel, T. A.; Tao, L.; Gao, F. *Nat. Commun.* **2015**, *6*, 8503.
- (42) Parvez, K.; Wu, Z.-S.; Li, R.; Liu, X.; Graf, R.; Feng, X.; Müllen, K. *J. Am. Chem. Soc.* **2014**, *136*, 6083.
- (43) Yang, S.; Brüller, S.; Wu, Z.-S.; Liu, Z.; Parvez, K.; Dong, R.; Richard, F.; Samori, P.; Feng, X.; Müllen, K. *J. Am. Chem. Soc.* **2015**, *137*, 13927.
- (44) Parvez, K.; Li, R. J.; Puniredd, S. R.; Hernandez, Y.; Hinkel, F.; Wang, S. H.; Feng, X. L.; Müllen, K. *ACS Nano* **2013**, *7*, 3598.
- (45) Shalu; Chaurasia, S. K.; Singh, R. K.; Chandra, S. *J. Phys. Chem. B* **2013**, *117*, 897.
- (46) Pech, D.; Brunet, M.; Taberna, P.-L.; Simon, P.; Fabre, N.; Mesnilgrente, F.; Conedera, V.; Durou, H. *J. Power Sources* **2010**, *195*, 1266.